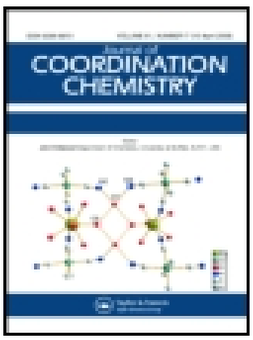

Journal of Coordination Chemistry

ISSN: 0095-8972 (Print) 1029-0389 (Online) Journal homepage: http://www.tandfonline.com/loi/gcoo20

Antimicrobial, antioxidant and SOD activities of copper(II) complexes derived from 2-aminobenzothiazole derivatives

J. Joseph, G. Boomadevi Janaki, K. Nagashri & R. Selwin Joseyphus

To cite this article: J. Joseph, G. Boomadevi Janaki, K. Nagashri & R. Selwin Joseyphus (2016): Antimicrobial, antioxidant and SOD activities of copper(II) complexes derived from 2-aminobenzothiazole derivatives, Journal of Coordination Chemistry, DOI: 10.1080/00958972.2016.1250153

To link to this article: http://dx.doi.org/10.1080/00958972.2016.1250153

Accepted author version posted online: 25 Oct 2016.

Publisher: Taylor & Francis
Journal: *Journal of Coordination Chemistry*
DOI: http://dx.doi.org/10.1080/00958972.2016.1250153

Antimicrobial, antioxidant and SOD activities of copper(II) complexes derived from 2-aminobenzothiazole derivatives

J. JOSEPH*†, G. BOOMADEVI JANAKI†, K. NAGASHRI‡ and R. SELWIN JOSEYPHUS§

†Department of Chemistry, Noorul Islam Centre for Higher Education, Kumaracoil-629 180, Tamil Nadu, India
‡Department of Chemistry, Renganayagi Varatharaj College of Engineering, Sivakasi, Tamilnadu, India
§Department of Chemistry, Mar Ivanios College, Trivandrum, Kerala, India

A series of Cu(II) complexes have been synthesized from bidentate Schiff base ligands (by condensation of Knoevenagel condensate of acetoacetanilide (obtained from substituted benzaldehydes and acetoacetanilide) and 2-aminobenzothiazole). They were characterized by elemental analysis, IR, ^{1}H-NMR, ^{13}C-NMR, UV-Vis., molar conductance, magnetic moment, ESR spectra and electrochemical studies. Based on the magnetic moment, ESR and electronic spectral data a distorted square planar geometry has been suggested for the complexes. Antibacterial and antifungal screening of the ligands and their complexes reveal that all the complexes show higher activities than the ligands. The antioxidant activities of the ligands and complexes were determined by superoxide and hydroxyl radical scavenging methods *in vitro*, indicating that the complexes exhibit more effective antioxidant activity than the ligands alone. The results show that the Cu(II) complexes also have similar superoxide dismutase activity to that of native Cu, Zn-SOD. All complexes exhibit suitable Cu(II)/Cu(I) redox potential ($E_{1/2}$) to act as synthetic antioxidant enzyme mimics.

Keywords: Bidentate; Geometry; ESR; Azomethine

Introduction

Most pharmaceutical agents contain transition metal as a constituent. Metals in therapeutic agents have become increasingly important, resulting in a variety of exciting and valuable drugs

*Corresponding author. Email: chem_joseph@yahoo.co.in

such as cis-platin for cancer, bismuth for ulcers, Gd for MRI contrasting agents, *etc*. Transition metal complexes of Schiff bases have attracted many researchers due to their biological activities such as antifungal, antibacterial, anticancer and herbicidal [1-5]. The complexation of metal to Schiff base ligand containing imine group improves the pharmacological activities of the ligand. Investigations on the interaction between transition metal complexes and DNA have attracted many researchers due to their importance in cancer therapy and molecular biology [6-9]. Schiff base metal complex is an attractive metal-based drug due to its special activities in pharmacology and physiology [10-12]. The coordination chemistry of copper(II) differs from other transition metals due to its size and electronic configuration. Copper is an important element present in several cell types with essential functions in the human body, participating in various biochemical processes [13, 14]. Complexes of copper with nitrogen or oxygen ligands are of considerable interest due to broad spectrum biological activities. Copper complexes, especially mononuclear copper complexes, are used as antifungal and antibacterial drugs, DNA structural probes, potential anticancer drugs and many neurodegenerative diseases, including atherosclerosis (heart disease and strokes), degenerative brain disorders, arthritis, cancers, *etc*.

In continuation of our research work, the present study focuses on synthesis and characterization of copper complexes of 2-aminobenzothiazole derivatives. The synthesized ligands and their copper complexes were subjected to antimicrobial activities using serial dilution technique.

Experimental

All chemicals used were of A.R. grade. Microanalytical data and FAB Mass spectra of the compounds were recorded. The amount of copper present in the copper complexes was estimated using ammonium oxalate method. NMR spectra of the ligands were recorded using TMS as internal standard. Chemical shifts are expressed in parts per million relative to TMS. The FAB mass spectra of the ligands and their complexes were recorded on a JEOL SX 102/DA-6000 mass spectrometer/data system using argon/xenon (6 kV, 10 mA) as the FAB gas. The accelerating voltage was 10 kV and the spectra were recorded at room temperature using *m*-nitrobenzylalcohol (NBA) as the matrix. IR spectra of the ligands and their copper complexes were recorded on a Perkin-Elmer 783 spectrophotometer from 4000-200 cm^{-1} using KBr discs. Electronic spectra were recorded with a Systronics 2201 Double beam UV-Vis.

spectrophotometer from 200-800 nm. The magnetic susceptibility values were calculated using the relation $\mu_{eff} = 2.83 (\chi m.T)^{1/2}$. The diamagnetic corrections were made by Pascal's constant and $Hg[Co(SCN)_4]$ was used as a calibrant. ESR spectra of the copper complexes were recorded at 300 and 77 K on a Varian E112 X-band spectrometer. Cyclic voltammetric measurements were performed on CHI 604D using a glassy carbon working electrode, Pt wire auxiliary electrode and a Ag/AgCl reference electrode. Tetrabutylammoniumperchlorate (TBAP) was used as the supporting electrolyte. All solutions were purged with N_2 for 30 min prior to each set of experiments. The X-ray diffractometer system JEOL JDX 8030 was used to record powder data for the copper complexes.

Preparation of Knoevenagel condensate β-ketoanilides

Ethanolic solution of 4-nitrobenzaldehyde (L^1)/benzaldehyde (L^2)/4-methoxybenzaldehyde (L^3) and 4-hydroxybenzaldehyde (L^4) was added to acetoacetanilide in a beaker with continuous stirring. The mixture was allowed to cool at room temperature and then piperidine was added to it drop by drop with constant stirring. Stirring was continued for further 10 min. Then the mixture was kept in a refrigerator for 48 h. After that the mixture was extracted with chloroform and 5% hydrochloric acid. The mixture was vigorously shaken in a separating funnel. The organic layer consists of Knoevenagel condensate β-ketoanilides and excess chloroform. The bottom layer was eluted and dried by magnesium sulphate to remove water. The excess chloroform was distilled out. The product was collected as orange yellow semi-solid and preserved in a dessicator.

Synthesis of Schiff base

Hot ethanolic solution of Knoevenagel condensate β-ketoanilides was refluxed with an ethanolic solution (30 mL) of 2-aminobenzothiazole and 1 g of anhydrous K_2CO_3 for about 12 h. The solvent was reduced to one-third and the pasty mass so obtained was treated with hot water and set aside in a refrigerator for 12 h. The solid material formed was removed by filtration and recrystallized from ethanol. Yield: 72%.

L^1: Yield: 72%. *Anal*. Calcd for $C_{31}H_{22}N_6S_2O_2$: C, 64.79; H, 3.86; N, 14.63. Found: C, 64.85; H, 3.92; N, 14.66. FAB mass spectrometry (FAB-MS): *m/z* 575 [M+1]. ^{1}H-NMR (400 MHz,

$CDCl_3$, δ, ppm): 6.4—7.5 (17H, m, Ar-H), 1.5 (3H, s, H3C-C), 5.8 (1H, s, aldehydic CH proton) and 11.2 (1H, s, N–H). ^{13}C-NMR (400 MHz, CDCl3, ppm): 10.1 (H3**C**-C), 18.9 (H**C**=C), 142.2 (**C**=CH), 152.8 (C-1), 122.5 (C-2), 116.8 (C-3), 153.9 (C-4), 117.7 (C-5), 145.8 (C-6), 122.5 (C-12), 125.8 (C-13), 156.2 (C-14), 120.1 (C-15), 132.5 (C-16), 126.3 (C-17), 143.8 (C-19), 124.2 (C-20), 120.5 (C-21), 123.8 (C-22), 124.1 (C-23), 125.4 (C-24), 143.8 (C-19′), 124.2 (C-20′), 120.5 (C-21′), 123.8 (C-22′), 124.1 (C-23′), 125.4 (C-24’), 172.6 (C-18), 172.6 (C-18′).

L^2: Yield: 58%. *Anal*. Calcd for $C_{31}H_{22}N_5S_2$: C, 66.01; H, 3.93; N, 12.42. Found: C, 66.05; H, 3.99; N, 12.48. FAB mass spectrometry (FAB-MS): *m*/*z* 576 [M+1]. ^{1}H-NMR (400 MHz, $CDCl_3$, δ, ppm): 6.8—7.9 (17H, m, Ar-H), 1.5 (3H, s, H3C-C), 5.6 (1H, s, aldehydic CH proton) and 11.8 (1H, s, N–H). ^{13}C-NMR (400 MHz, CDCl3, ppm): 10.8 (H3**C**-C), 20.4 (H**C**=C), 146.4 (**C**=CH), 153.6 (C-1), 120.5. (C-2), 116.8 (C-3), 153.9 (C-4), 117.7 (C-5), 145.8 (C-6), 123.1 (C-12), 125.6 (C-13), 156.2 (C-14), 124.6 (C-15), 156.2 (C-16), 125.6 (C-17), 143.8 (C-19), 124.2 (C-20), 120.5 (C-21), 123.8 (C-22), 124.1 (C-23), 125.4 (C-24), 143.8 (C-19′), 124.2 (C-20′), 120.5 (C-21′), 123.8 (C-22′), 124.1 (C-23′), 125.4 (C-24’), 172.6 (C-18), 172.6(C-18′).

L^3: Yield: 66%. *Anal*. Calcd for $C_{31}H_{23}N_5S_2O$: C, 68.24; H, 4.25; N, 12.52. Found: C, 68.32; H, 4.36; N, 12.60. FAB mass spectrometry (FAB-MS): *m*/*z* 546 [M+1]. ^{1}H-NMR (400 MHz, $CDCl_3$, δ, ppm): 6.4—7.5 (9H, m, Ar-H), 1.5 (3H, s, H3C-C), 1.8 (3H, s, aldehydic CH proton) and 11.2 (1H, s, N–H). ^{13}C-NMR (400 MHz, CDCl3, ppm): 11.8 (H3**C**-C), 19.5 (H**C**=C), 144.4 (**C**=CH), 152.8 (C-1), 122.5 (C-2), 116.8 (C-3), 153.9 (C-4), 117.7 (C-5), 145.8 (C-6), 123.8 (C-12), 126.9 (C-13), 156.8 (C-14), 121.6 (C-15), 133.4 (C-16), 126.9 (C-17), 143.8 (C-19), 124.2 (C-20), 120.5 (C-21), 123.8 (C-22), 124.1 (C-23), 125.4 (C-24), 143.8 (C-19′), 124.2 (C-20′), 120.5 (C-21′), 123.8 (C-22′), 124.1 (C-23′), 125.4 (C-24’), 172.6 (C-18), 172.6 (C-18′).

L^4: Yield: 62%. *Anal*. Calcd for $C_{32}H_{25}N_5S_2O$: C, 68.68; H, 4.51; N, 12.52. Found: C, 68.78; H, 4.65; N, 12.61. FAB mass spectrometry (FAB-MS): *m*/*z* 560 [M+1]. ^{1}H-NMR (400 MHz, $CDCl_3$, δ, ppm): 6.4—7.5 (9H, m, Ar-H), 1.5 (3H, s, H3C-C), 1.8 (3H, s, aldehydic CH proton) and 11.2 (1H, s, N–H). ^{13}C-NMR (400 MHz, CDCl3, ppm): 10.9 (H3**C**-C), 19.9 (H**C**=C), 142.6 (**C**=CH), 152.8 (C-1), 122.5 (C-2), 116.8 (C-3), 153.9 (C-4), 117.7 (C-5), 145.8 (C-6), 123.9

(C-12), 126.2 (C-13), 156.7 (C-14), 120.8 (C-15), 133.9 (C-16), 127.0 (C-17), 143.8 (C-19), 124.2 (C-20), 120.5 (C-21), 123.8 (C-22), 124.1 (C-23), 125.4 (C-24), 143.8 (C-19′), 124.2 (C-20′), 120.5 (C-21′), 123.8 (C-22′), 124.1 (C-23′), 125.4 (C-24'), 172.6 (C-18), 172.6 (C-18′).

Synthesis of copper(II) complexes

An ethanolic solution of L^1-L^4 was added to a solution of copper acetate in ethanol (20 mL) and the mixture was refluxed for 1 h, concentrated to one-third volume and kept at 0 °C for 2 h. The solid product formed was filtered, washed several times with small amounts of ethanol and diethyl ether and dried in vacuo. Yield: 64%.

Complex of L^1: Yield: 62%. *Anal*. Calcd for $CuC_{37}H_{32}N_6O_6$: C, 56.65; H, 4.11; N, 10.72, Cu, 8.11. Found: C, 56.68; H, 4.17; N, 10.78; Cu, 8.17. FAB mass spectrometry (FAB-MS), *m*/*z* 785 [M+1]. μ_{eff} (BM) = 1.90; Λ_m (S cm^2 mol^{-1}) = 08.

Complex of L^2: Yield: 66%. *Anal*. Calcd for $CuC_{37}H_{32}N_5O_4$: C, 57.42; H, 4.17; N, 9.06, Cu, 8.22. Found: C, 57.48; H,4.24; N, 9.15; Cu, 8.27. FAB mass spectrometry (FAB-MS), *m*/*z* 775 [M+1]. μ_{eff} (BM) = 1.92; Λ_m (S cm^2 mol^{-1}) = 12.

Complex of L^3: Yield: 72%. *Anal*. Calcd for $CuC_{37}H_{33}N_5O_5$: C, 58.83; H, 4.41; N, 9.28, Cu, 8.42. Found: C, 58.92; H, 4.16; N, 9.34; Cu, 8.53. FAB mass spectrometry (FAB-MS), *m*/*z* 756 [M+1]. μ_{eff} (BM) = 2.02; Λ_m (S cm^2 mol^{-1}) = 06.

Complex of L^4: Yield: 70%. *Anal*. Calcd for $CuC_{38}H_{35}N_5OS_2$: C, 59.32; H, 4.59; N, 9.11; Cu, 8.27. Found: C, 74.62; H, 4.63; N, 9.19; Cu, 8.31. FAB mass spectrometry (FAB-MS), *m*/*z* 770 [M+1]. μ_{eff} (BM) = 1.96; Λ_m (S cm^2 mol^{-1}) = 10.

Antimicrobial activity

The *in vitro* antimicrobial activities of the investigated compounds were tested against the bacterial species, *Staphylococcus aureus* (ATCC 25923), *Escherichia coli* (ATCC 25922), *Klebsiella pneumaniae* (ATCC 2473), *Proteus vulgaris* (ATCC 8427) and *Pseudomonas aeruginosa* (ATCC 27853) and fungal species *Aspergillus niger* (ATCC 16888), *Rhizopus*

stolonifer (ATCC 14037), *Aspergillus flavus* (ATCC 9643), *Rhizoctonia bataicola* (ATCC 14016) and *Candida albicans* (ATCC 10231) by disc diffusion method. MIC is the lowest concentration of an antimicrobial compound that will inhibit the visible growth of a microorganism after overnight incubation. MIC of the various compounds against bacterial strains was tested through a modified agar well diffusion method.

Antioxidant assay

The samples were tested individually at a final concentration of 10 μM. The solution contained 1 mL of DPPH (diphenylpicrylhydrazyl radical, 60 μM) and different concentrations of the antioxidant solutions of ligands and their complexes, resulting in a final concentration of DPPH of 30 μM. The mixtures were vigorously mixed and allowed to stand in the dark for 30 min at 25 °C. The absorbances of the resulting solutions were measured at 517 nm against a blank sample containing only DPPH, the negative control; Rutin and Vitamin C served as positive controls.

$$\text{Scavenging effect (\%)} = ((A_0-A_1) / A_0) \times 100 \qquad (1)$$

where A_0 is the absorbance of the control reaction and A_1 is the absorbance in the presence of the samples or standards.

Inhibition of superoxide radicals by riboflavin photoreduction method

Superoxide scavenging was determined by the NBT reduction method. The reaction mixture containing EDTA (0.1M), 0.0015% NaCN, riboflavin (0.12 mM), NBT (1.5 mM) and various concentrations of test sample and total volume was adjusted by adding phosphate buffer (6.7 mM, pH 7.8) to 3 mL in a test tube. The tubes were uniformly illuminated under an incandescent lamp for 15 minutes, and thereafter the optical density was measured at 530 nm. The percentage inhibition of superoxide production was evaluated by comparing the absorbance of the control and experimental tubes. The percentage inhibition was calculated by using the formula

$$\text{Percentage inhibition} = ((C-T) \times 100) / C$$

where C and T are the optical density of the control and test samples, respectively.

DNA binding

Thermal denaturation (T_m) studies

Thermal denaturation studies were performed on a Systronics spectrophotometer equipped with a thermostatic cell holder. The T_m value of CT-DNA was determined in the absence and presence of Cu(II) complexes by keeping the concentration of DNA and $[Cu(L^{10})(H_2O)]$ (30 µM) in a 1:1 ratio. The DNA samples were continuously heated at 1 °C/min, while the absorption changes at 260 nm were monitored. The melting temperature (T_m), which is defined as the temperature where half of the total base pairs are unbound, was determined from the midpoint of the melting curves. ΔT_m values were calculated by subtracting T_m of free DNA from T_m of DNA interacting with the complex.

UV–Vis absorption spectroscopy

Absorption spectra were recorded on a Systronics 2201 Double beam UV-Vis. spectrophotometer using 1 cm quartz micro-cuvettes. Absorption titrations were performed by keeping the concentration of the complexes constant (10 µM), and by varying the concentration of CT-DNA from 0 to 10 µM. In the reference cell, a DNA blank was placed so as to cancel any absorbance due to DNA at the measured wavelength. For $[Cu(L^{10})(H_2O)]$ the binding constants (K_b) were determined from the spectroscopic titration data using the following equation:

$$[DNA]/(\varepsilon_a-\varepsilon_f) = [DNA]/(\varepsilon_b-\varepsilon_f)+ 1/(\varepsilon_a-\varepsilon_f)$$

The 'apparent' extinction coefficient (ε_a) was obtained by calculating $A_{obsd}/[Cu]$. The terms (ε_f) and (ε_b) correspond to the extinction coefficients of free (unbound) and the fully bound complexes, respectively. A plot of $[DNA]/(\varepsilon_a-\varepsilon_f)$ versus [DNA] will give a slope of $1/(\varepsilon_a-\varepsilon_f)$ and an intercept of $1/K_b(\varepsilon_a-\varepsilon_f)$. K_b is the ratio of the slope to the intercept.

Electrochemical studies

Electrochemical behavior of copper complexes was recorded at room temperature in a CHI 604D Electrochemical analyzer. Cyclic voltammetric measurements were performed using a glassy

carbon working electrode, Pt wire auxiliary electrode and a Ag–AgCl reference electrode. Tetrabutylammonium perchlorate was used as the supporting electrolyte. All solutions were purged with N_2 for 30 min prior to each set of experiments. The electrochemical behavior of the Cu(II) complexes in DMSO were performed in the presence and absence of CT DNA.

Partition coefficient determination

The lipophilicities of the complexes were determined by the shake flask method using phosphate buffer (0.12 M NaCl) and *n*-octanol. Each compound was dissolved in the phase in which duplicate determinations using three different solvent ratios were performed for each complex. Following mixing and phase separation according to literature methods, each phase was analyzed for solute content and the concentration was determined using spectrophotometric methods. All *n*-octanol/water partition coefficients were determined by UV-visible spectroscopy. Octanol and buffer solutions were pre-saturated with each other prior to use.

3. Results and discussion

The synthetic routes of the ligands (obtained from the condensation of Knoevenagel condensate β-ketoanilides and 2-aminobenzothiazole) and their corresponding copper(II) complexes have been outlined in scheme 1. They were thoroughly characterized by elemental analyses and various analytical and spectroscopic techniques to identify their formulas to elucidate molecular structures of ligands and their copper complexes. The purity of ligands and their copper complexes has been checked by TLC. The analytical data provided in the Experimental section for the ligands and their complexes were in agreement with the molecular formulas $[Cu(L)(OAc)_2]$. All the compounds are stable at room temperature in the solid state without decomposition. The melting points of the complexes are higher than that of the ligands revealing that the complexes are more stable than the ligands.

The ligands are more soluble in common polar organic solvents, such as $CHCl_3$, EtOH and THF, but partially soluble in nonpolar organic solvents, such as hexane, heptane and toluene. The complexes are soluble only in polar organic solvents, such as DMF and DMSO. The observed low molar conductance values of the copper complexes are consistent with non electrolytes. Therefore, acetate is bonded to copper. The IR peak shift in $\nu_{C=N}$ of the ligand in the complexes gave an idea about its coordination to copper(II). The geometry around Cu(II)

has been deduced from the absorption band observed in the UV–Vis spectra and magnetic moment values.

Conductometric measurements in DMSO solution of the complexes showed no significant change in the conductivity in comparison with that of the pure solvents. This behavior is in agreement with the neutrality of the complexes, according to the formula assigned. The conductivities of DMSO solutions were measured during a week and no major changes were observed in solvents, showing the stability of the complexes in these solvents.

IR spectra

IR spectra provide information regarding the nature of the functional group attached to copper. IR spectra of L^1 and its copper complex are shown in figure 1. The spectrum of the ligand showed two different -C=N bands from 1646-1681 cm^{-1}, which are shifted to lower frequencies in spectra of all the complexes (1580-1634 cm^{-1}), indicating involvement of ν(-C=N) nitrogen in coordination to copper. The present ligand systems are bidentate, bonded to copper ion *via* two nitrogens (-C=N) of the Schiff base. New bands at 456 cm^{-1} and 514 cm^{-1} correspond to ν(M-N) and ν(M-O) [15]. Also bands at 1386 cm^{-1} and 1290 cm^{-1} correspond to symmetric and asymmetric ν(M-O), evidence for participation of COO^- ion in the complexes. These facts are further supported by appearance of bands between 1394-1458 cm^{-1} and 1282-1328 cm^{-1} attributed to $\upsilon_{asy}(COO^-)$ and $\upsilon_{sy}(COO^-)$, respectively, in all copper complexes. The difference in Δυ between $\upsilon_{asy}(COO^-)$ and $\upsilon_{sy}(COO^-)$ in metal complexes was ~100 cm^{-1} (110-135 cm^{-1}) suggesting coordination of carboxylate is monodentate. Thus copper complexes were coordinated through azomethine nitrogens and acetates. The IR spectral features reinforced the conclusion drawn from conductance measurements [16].

Electronic absorption spectra

Electronic absorption spectra of ligands and their complexes were recorded at 300 K in DMSO and presented in the Experimental section. L^1 shows two bands at 352 nm and 245 nm which may be assigned to $n\rightarrow\pi^*$ and $\pi\rightarrow\pi^*$ transitions, respectively. The electronic spectrum of $[CuL^1(OAc)_2]$ shows a shoulder of CT-transition at 320 nm and a broad d–d absorption centered at 584 nm, due to $^2B_{1g}\rightarrow{}^2A_{1g}$ as reported for square planar Cu(II) complexes. The room temperature magnetic moment for copper complexes (μ_{eff} = 1.75 BM) falls in the normal range

for copper(II) species with S = 1/2 and confirms that the copper(II) complex has square-planar geometry with $d_{x^2-y^2}$ ground state.

UV spectra of the complexes have been recorded in the pH range 6-8 (biological experiments are performed at pH = 7) with the use of different buffer solutions (150 mM NaCl and 15 mM trisodium citrate at pH values regulated by HCl solution) and no significant changes (shift of the absorption or new absorption peaks) occurred, indicating that the complexes are stable in the pH range 6-8. They showed similar UV-Vis spectral pattern in DMSO solution, in the presence of the buffer solution (150 mM NaCl and 15 mM trisodium citrate in the pH = 7.0) used in the biological experiments and in the pH range 6-8 suggesting that the compounds are stable in solution.

NMR spectra

The ^{1}H NMR spectra of ligands were recorded in DMSO-d_6 and the data along with the assignments are summarized in the Experimental section. NMR spectra of the Cu(II) complexes are less resolved than that of the ligand due to broadening from paramagnetic properties of the compound. The data obtained from the elemental analyses, IR, and ^{1}H NMR spectral measurements are in agreement with each other.

FAB mass spectra

The FAB mass spectra of the ligands and their copper complex were recorded and compared for stoichiometric compositions. FAB mass spectrum of copper complex of L^1 is shown in figure 2. The molecular ion peak for L^1 is observed at 575 m/z ratio which is also supported by the "Nitrogen Rule", since the compound possesses an even number of nitrogens. The molecular ion peak for the copper complex was observed at m/z = 785, confirming the stoichiometry of copper chelates as $[CuL^1(OAc)_2]$ type. It is also supported by FAB mass spectra of the other complexes. The proposed path of the decomposition for the investigated Schiff base is presented in scheme 2. Microanalytical data are also in agreement with values calculated from molecular formulas assigned to these complexes, which is further supported by the FAB-mass studies of representative complexes. The mass spectral features reinforced the conclusion drawn from elemental analysis, copper estimation and molar conductance values.

ESR spectra

EPR spectra of the Cu(II) complexes have been recorded at room temperature as well as at liquid nitrogen temperature and their g_{II} and $g_{\perp}$ values calculated. The data show that g_{II} = 2.085–2.219 and $g_{\perp}$ = 2.018–2.046 (table 1). The values of g_{II} and $g_{\perp}$ are close to 2 and $g_{II} > g_{\perp}$. This suggests that the unpaired electron is in the $d_{x^2-y^2}$ orbital and hence, $^2B_1$ is the ground state. For an ionic environment $g_{II} > 2.3$, while for a covalent environment $g_{II} < 2.3$. The copper complexes show $g_{II} < 2.3$ indicating considerable covalent character. The g values are related by the expression $G = (g_{II} - 2)/(g_{\perp} - 2)$ which suggests an exchange interaction between copper centers in the polycrystalline solid. If G > 4, the exchange interaction is negligible. In the present case, the axial symmetry parameter, G, is 4.025–5.896, which indicates no significant exchange interaction in these solid complexes.

The EPR spectra of copper(II) complexes were recorded in DMSO at 300 and 77 K. The 300 K spectrum shows an isotropic pattern, expected for Cu^{2+} in solution, but the spectra for the frozen solutions show the usual anisotropic pattern expected for a powder sample. The absence of half field signal at 1600 G, corresponding to $\Delta Ms = \pm 2$ transition, rules out any Cu-Cu interaction in the EPR spectra [17]. The spin Hamiltonian parameters of the complexes are given in table 1. The frozen DMSO solution is axial with $g_{II} > g_{\perp} > 2.0023$, indicating a $d_{x^2-y^2}$ ground state [18] which is in agreement with the electronic absorption spectroscopic assignments. The frozen solution spectrum of the complex shows four-line hyperfine splitting A_{II} with signals from ^{63}Cu and ^{65}Cu slightly resolved at the low field component. The most remarkable feature is that the g_{II} value (2.18-2.24) is substantially higher than the majority of known copper(II) complexes. A factor potentially contributing to increase of g_{II} is distortion from square-planar geometry [19].

The electron spin resonance and optical spectra have been used to determine the covalent bonding parameters for Cu(II) in various ligand field environments. Since there has been interest in the nature of bonding parameters in the system, we adopted simplified molecular orbital theory to calculate the bonding coefficients such as in-plane σ-bonding (α^2), out-plane π-bonding (β^2) and in-plane π-bonding (γ^2). The observed α^2 (less than unity) and β^2 (greater than 0.5) values indicate that the copper(II) complexes have some covalent character.

The degree of geometrical distortion was described by a parameter; $f = g_{//}/A_{//}$ is an index of tetragonal distortion. The f values less than 135 are associated with the square-planar structures, whereas higher values indicate distortions towards tetrahedra [20]. The f values of

complexes were 126–141, indicating significant distortion from planarity. The nature of ligand moieties and functional groups (in the ligands) influenced distortion from planarity. For the present complexes, the g_{II}/A_{II} is 143-145, in agreement with significant deviation from planarity and which is further confirmed by the bonding parameter α^2 whose value is less than unity.

Redox behavior

The electrochemical behavior of the Cu(II) complexes in DMSO (0.1 M of TBAP as supporting electrolyte, scan rate 100 mV s^{-1} at 300 K) were examined and tabulated (table 2). The cyclic voltammogram of $[CuL^1(OAc)_2]$ in DMSO solution at 300 K in the potential range +0.8 to -0.8 V at scan rate 0.1 Vs^{-1} is shown in figure 3. It shows a well-defined redox process corresponding to the formation of the quasi-reversible Cu(II)/Cu(I) couple. The anodic peak at Epa = -0.602 mV versus Ag/AgCl and the associated cathodic peak at Epc = -0.746 mV correspond to the Cu(II)/Cu(I) couple. $[CuL^1(OAc)_2]$ exhibits quasi-reversible behavior. It also shows one irreversible peak at 0.416 mV which was assigned to Cu(II)/Cu(III). Similar electrochemical behavior was observed for other complexes.

On comparing the cyclic voltammograms, we observed that the variation in oxidation and reduction potential may be due to distortion in the geometry of the complexes which arises due to different donors coordinated to copper. The present ligand systems stabilize the unusual oxidation states of copper ion during electrolysis. The separation between the cathodic and anodic peak current (I = Ipa/Ipc = 1.1) indicates a quasi reversible one electron process assignable to Cu(II)/Cu(I) couple.

Substitution effects

Ligands containing unsaturated nitrogens and sulfur have been shown to facilitate reduction of Cu(II) to Cu(I). Karlin suggested that copper sites in metalloproteins exhibit geometries that favor Cu(I) [21]. The nature and position of substituents have also been shown to affect the value of the redox potentials of the Cu(II)/Cu(I) couple. In the present study, the copper complexes of substituted Knoevenagel condensates contain 2-aminobenzothiazole. The observed redox potential of the Cu(II)/Cu(I) couple is controlled by the molecular structures of the complexes, which depend on the substituents present in the ligands. The introduction of electron-withdrawing substituent at the 4-position in the Knoevenagel condensates produced an increase

in the redox potential compared to that of the electron-releasing substituents. The electrochemical behaviors of copper complexes in DMSO solutions were measured and are summarized in table 2.

Powder XRD study

In absence of single crystal, X-ray powder data are useful to deduce accurate cell parameters. The diffraction pattern reveals the crystalline nature of the complex. The crystallite sizes of the copper complexes were calculated from Scherre's formula. The appearance of crystallinity in the Cu(II) complex is due to the inherent crystalline nature of the copper complexes (table 3). The powder XRD pattern of the copper complex of L^1 is shown in figure 4.

Solvatochromism

The electronic absorption spectra of copper complexes were performed in different solvents. The structural characteristics of copper complexes are: (i) their high solubility in various organic solvents and (ii) the change in the color of the solution on going from one solvent to another, *i.e.*, strong solvatochromism of their solutions. The spectra showed one broad band which corresponds to promotion of the electron in the lower energy orbital to the hole in $d_{x^2-y^2}$ orbital of copper(II) (d^9). The position of this band shifted to longer wavelength (red shift) as the polarity of solvent increases. Therefore, the copper complex structure depends on the polarity of solvents.

Antimicrobial study

The *in vitro* antimicrobial activities of the investigated compounds were tested against bacterial and fungal species. The minimum inhibitory concentration (MIC) values of the compounds are summarized in tables 4 and 5. A comparative study of the ligands and their complexes (MIC values) indicates that complexes exhibit higher antimicrobial activity than the free ligands. The activity of the Schiff base ligands may arise from hydroxyl groups, which play an important role in antibacterial activity, as well as the presence of two imine groups important in elucidating the mechanism of transformation in biological systems. The obtained results indicate that the complexes have higher activity than the ligands against the same microorganisms under identical experimental conditions, suggesting that chelation could facilitate a complex to cross a cell membrane and can be explained by Tweedy's chelation theory [22, 23]. The variation in the

effectiveness of different compounds against different organisms depends either on the impermeability of the cells of the microbes or on differences in ribosome of microbial cells. The activity of the Schiff base ligands and their metal complexes increases as the concentration increases. The activity of complexes may be due to the effect of the acetate ions. These complexes disturb the respiration process of the cell and thus block the synthesis of proteins restricting further growth of the organism and as a result microorganisms die.

The prepared complexes were more active against Gram-positive than Gram-negative bacteria, indicating that the antimicrobial activity of the compounds is related to cell wall structure of the bacteria. The cell wall is essential to the survival of bacteria and some antibiotics are able to kill bacteria by inhibiting a step in the synthesis of peptidoglycan. Gram-positive bacteria possess a thick cell wall containing many layers of peptidoglycan and teichoic acids, but Gram negative bacteria have a relatively thin cell wall consisting of a few layers of peptidoglycan surrounded by a second lipid membrane containing lipopolysaccharides and lipoproteins. These differences in cell wall structure can produce differences in antibacterial susceptibility and some antibiotics can kill only Gram-positive bacteria and are ineffective against Gram-negative pathogens. This higher antimicrobial activity of the copper complexes may be ascribed to electronic and/or structural changes of the ligated molecules due to coordination, making the metal complexes more powerful bacteriostatic agents, thus inhibiting the growth of the microorganisms.

Absorption spectral features of DNA binding

DNA binding studies of the complexes were studied using absorption spectra. A complex bound to DNA through intercalation is characterized by change in absorbance (hypochromism) and red shift in wavelength due to intercalation involving a strong stacking interaction between the aromatic substituent and the DNA base pairs. The extent of hypochromism is consistent with the strength of the intercalative interaction.

After interaction with the base pairs of DNA, the $\pi \rightarrow \pi^*$ orbital of the bound ligand can couple with the π orbital of the base pairs, due to decrease in $\pi \rightarrow \pi^*$ transition energy, which results in bathochromic shift. The results show that the absorbance (hypochromism) decreased with successive addition of CT-DNA to the complex solution.

Hypochromism and bathochromic shift are observed for the complexes, suggesting that binding is intercalative. The observed K_b values for copper complexes are equal to classical intercalators bound to CT-DNA. The K_b values for the complexes are 4.4×10^6 M^{-1}, 3.2×10^6 M^{-1}, 2.8×10^6 M^{-1} and 3.6×10^6 M^{-1}, respectively. The values of K_b have been described in the literature for classical intercalators (ethidium bromide–DNA) whose binding constant have been found to be in the order of 10^7 M^{-1}. The results show that the present complexes are involved in intercalative interactions with CT-DNA.

Viscosity measurements

The nature of the interaction between the complexes and CT-DNA were determined by viscosity measurements. A classical intercalative mode was obtained on the basis of increase in viscosity of DNA solution due to an increase in separation of base pairs at the intercalation sites and increase in DNA length. Hydrodynamic measurements are sensitive to length change (*i.e.* viscosity and sedimentation) are critical tests of a binding model in solution in the absence of crystallographic structural data. A classical intercalation model demands that the DNA helix must lengthen as base pairs separate. The plots of $(\eta/\eta_o)^{1/3}$ *vs* [Complex]/[DNA] (η and η_o are the relative viscosities of DNA in the presence and absence of compound, respectively) gives a measure of the viscosity changes. On increasing amounts of complexes, the relative viscosity of DNA increases steadily, similar to the behavior of ethidium bromide. The result shows that metal complexes intercalate between the base pair of DNA, consistent with spectroscopic results.

Thermal denaturation studies

Thermal denaturation studies show evidence for the ability of the complexes to stabilize the double-stranded DNA. Interactions between DNA and complexes were indicated by increase in the thermal melting temperature (T_m). Thermal denaturation experiments also revealed intercalation of these metal complexes with DNA. When the temperature increases in solution, the double-stranded DNA dissociates to single strands and generates a hypochromic effect on the absorption spectra of DNA bases (λ_{max} = 260 nm). The extinction coefficient of the DNA base at 260 nm in the double-helical form is much less than that in the single strand form; hence, melting of the helix leads to an increase in the absorption at this wavelength. Thus, the helix to coil transition temperature can be determined by monitoring the absorbance of the DNA bases at λ_{max}

= 260 nm as a function of temperature. This transition process, the melting temperature T_m, defined as the temperature where half of the total base pairs are bonded, is introduced. The T_m of calf thymus DNA is 65.8 ± 0.2 °C. Under the same set of conditions, addition of metal complexes increased T_m by 1 °C, 2 °C and 3 °C, respectively, which indicate that these compounds stabilize the double helix of DNA. This method is easy to identify when more than one transition occurs. This transition of double stranded DNA to single stranded DNA is termed as the melting temperature of DNA (T_m). These variations in T_m of calf thymus DNA strongly supported intercalation of metal complex into double helix DNA.

SOD activity

To correlate the structural aspects with the SOD activity, EPR spectra of both complexes were recorded at 77 K in DMSO. Diaz *et al*. [24] have reported a good correlation between f factor (g_{ll}/A_{ll}, where A_{ll} is expressed in cm^{-1}) and SOD like activity, for a series of Cu(II) complexes. An f factor value smaller than 135 cm is obtained for square planar Cu(II) complexes, and this value increases with increasing square planar distortion. The f value for native SOD is 160 cm, indicating a tetrahedral distortion from square planar geometry, which is one of the features that enhances the catalytic activity of the enzyme. From the above EPR data, the f values for 1:1 complexes were determined to be 150, 145, 142 and 135 cm, respectively.

During SOD activity, there is change in the oxidation state from Cu(II) to Cu(I). Partially filled orbitals get extra stabilization due to Crystal Field Stabilization Energy (CFSE) during the complex formation process, whereas completely filled orbitals tend to have a tetrahedral geometry which will have minimum ligand-ligand repulsion. Thus flexible ligands around the Cu ion will help to shuttle between different oxidation states. The copper complexes exhibiting appreciable square planar distortion are expected to show higher SOD activity.

Synthetic SOD mimics should be designed by taking into consideration longer shelf life, higher lipid solubility and penetration into cells. It would be preferable to have SOD mimic redox active metal complexes with antioxidants and other inflammatory drugs, because of added pharmacological activity and reduced toxicity of the ligands. Curcumin has a remarkable pharmacological activity including anti-inflammatory, anticarcinogenic and antioxidant activity with almost no side effects. We hoped that the proposed copper complexes had higher biological activity and behaved as synthetic enzyme mimic agents.

Antioxidant

Antioxidants that exhibit DPPH radical scavenging activity have received attention. Compounds with antioxidant properties could be expected to offer protection in rheumatoid arthritis and inflammation and lead to potentially effective drugs. Copper complexes of L^3 showed good antioxidant activity due to the presence of OH group and efficient hydrogen donors to stabilize the unpaired electrons and thereby scavenge free radicals. The introduction of OH group in the ligand system markedly increases the antioxidant efficiency of the complexes with careful selection of the substituents on the ligand, the antioxidant behavior of the complexes can be improved.

Partition coefficient determination

Partition coefficients, P, were measured to find the capacity of organic/inorganic based compounds to cross lipid layers and inhibit microbial growth. The synthesized compounds were tested for partition coefficients using the shake flask method. The synthesized compounds have different P values due to conjugated system and different substituents present in the compounds. The synthesized ligands have LogP values between 4.4-6.8, suggesting that ligands have liphophilic characteristics.

The biosensitive copper complexes were subjected to the shake flask method to find the partition coefficients, LogP in the range 3.4-4.2. Copper complex containing electron-withdrawing substituent in L^1 has low LogP value compared to other complexes. This liphophilic behavior suggested that the complexes may penetrate more efficiently across the lipoidal bacterial membrane than free ligands. These complexes may behave as effective chemotherapeutic drugs after clinical trials.

Oxidative damage

The oxidative damage of HSA along with copper complexes in the presence of H_2O_2 was performed at room temperature for 30 min (incubation). It was observed that copper complex was able to cause extensive protein degradation after incubation with H_2O_2. In the incubation period, the generation of hydroxyl radical is responsible for the observed degradation. The hydroxyl radical mediated protein degradation in the presence of copper complex was confirmed

using Rhodamine B dye test. The solution containing hydroxyl radical which degrades Rhodamine B dye during incubation with HAS and copper complex was monitored using UV-Vis spectroscopy.

Conclusion

Bidentate Schiff base ligands derived from Knoevenagel condensate β-ketoanilides (obtained from acetoacetanilide and benzaldehyde) and 2-aminobenzothiazole and their copper(II) complexes were characterized by analytical and spectral techniques. From the electronic absorption spectra and ESR spectral data, a distorted square-planar geometry was assigned for the complexes. The lower conductivity values indicated that all the complexes are non-electrolytes. Based on their magnetic susceptibility and ESR spectral data, monomeric complexes were confirmed. The redox properties of copper ion, azomethine (>C=N) group, hydroxyl moiety and also heterocyclic moieties are responsible for increased antimicrobial activity. The new derivatives may provide choice and flexibility to change the structure in order to find a less toxic derivative with enhanced activity. Copper complex of L^1 presents a promising pharmacological profile that could be an interesting starting point for future chemical modifications in order to improve activity.

Acknowledgements

We express our sincere thanks to the Professor and Head, Department of Chemistry, and the management of Noorul Islam Centre for Higher Education, Kumaracoil for their constant encouragement and providing research facilities. JJ also thanks DST, New Delhi for financial assistance (YSS/CS-029/2013).

References

[1] P.J. Ferguson, E.M. Kurowska, D.J. Freeman, A.F. Chambers, J. Korpatnick. *Nutr. Cancer*, **56**, 86 (2006).

[2] G.S. Sim, B.C. Lee, H.S. Cho. *Arch. Pharmacol. Res.*, **30**, 290 (2007).

[3] N. Bharti, R.M. Maurya, F. Naqvi, A. Bhattacharya, S. Bhattacharya, A. Azam. *Eur. J. Med. Chem.*, **35**, 481 (2000).

[4] N.L. Wengnack, H.M. Hoard, F. Rusnak. *J. Am. Chem. Soc.*, **121**, 9748 (1999).

[5] M.R. Maurya. *Coord. Chem. Rev.*, **237**, 163 (2003).

[6] F. Mohamadon, J.P. Barbier, R.P. Hugel. *Polyhedron*, **11**, 2697 (1992).

[7] A.E. Liberta, D.X. West. *BioMetals*, **5**, 121 (1992).

[8] A. Cole, P.M. May, D.R. Williams. *Agents Actions*, **11**, 296 (1992).

[9] K. Singh, M.S. Barwa, P. Tyagi. *Eur. J. Med. Chem.*, **42**, 394 (2007).

[10] J. Lv, T. Liu, S. Cai, X. Wang, L. Liu, Y. Wang. *J. Inorg. Biochem.*, **100**, 1888 (2006).

[11] J.R.J. Sorenson. *J. Med. Chem.*, **19**, 135 (1976).

[12] P. Kamalakannan, D. Venkappayya. *J. Inorg. Biochem.*, **21**, 22 (2002).

[13] M.L. Dhar, M.M. Dhar, B.N. Dhavan, B.N. Mehrotra, C. Ray. *Indian J. Exp. Biol.*, **6**, 232 (1968).

[14] L.A. Collins, S.G. Franzblau. *Antimicrob. Agents Chemother.*, **41**, 1004 (1997).

[15] W.J. Geary. *Coord. Chem. Rev.*, **7**, 81 (1971).

[16] K. Nakamoto, *Infrared Spectra of Inorganic and Coordination Compounds*, Wiley, New York (1970).

[17] B.J. Hathaway, D.E. Billing. *Coord. Chem. Rev.*, **5**, 143 (1970).

[18] D.E. Billing, B.J. Hathaway, P. Nicholls. *J. Chem. Soc. (A)*, 316 (1969).

[19] N. Raman, A. Kulandaisamy, C. Thangaraja. *Transition Met. Chem.*, **29**, 129 (2004).

[20] K. Nagashri, J. Joseph, C.J. Dhanaraj. *Appl. Organomet. Chem.*, **25**, 704 (2011).

[21] K.H. Reddy, P.S. Reddy, P.R. Babu. *J. Inorg. Biochem.*, **11**, 169 (1999).

[22] R. Malhotra, S. Kumar, K.S. Dhindsa. *Indian J. Chem.*, **32A**, 457 (1933).

[23] R.S. Srivastava. *Inorg. Chim. Acta*, **56**, 65 (1944).

[24] M.N. Diaz, B. Frei, J.A. Vita, J.F. Keaney, Jr. *New Engl. J. Med.*, **337**, 408 (1997).

Scheme 1. Systematic route for synthesis of copper complex.

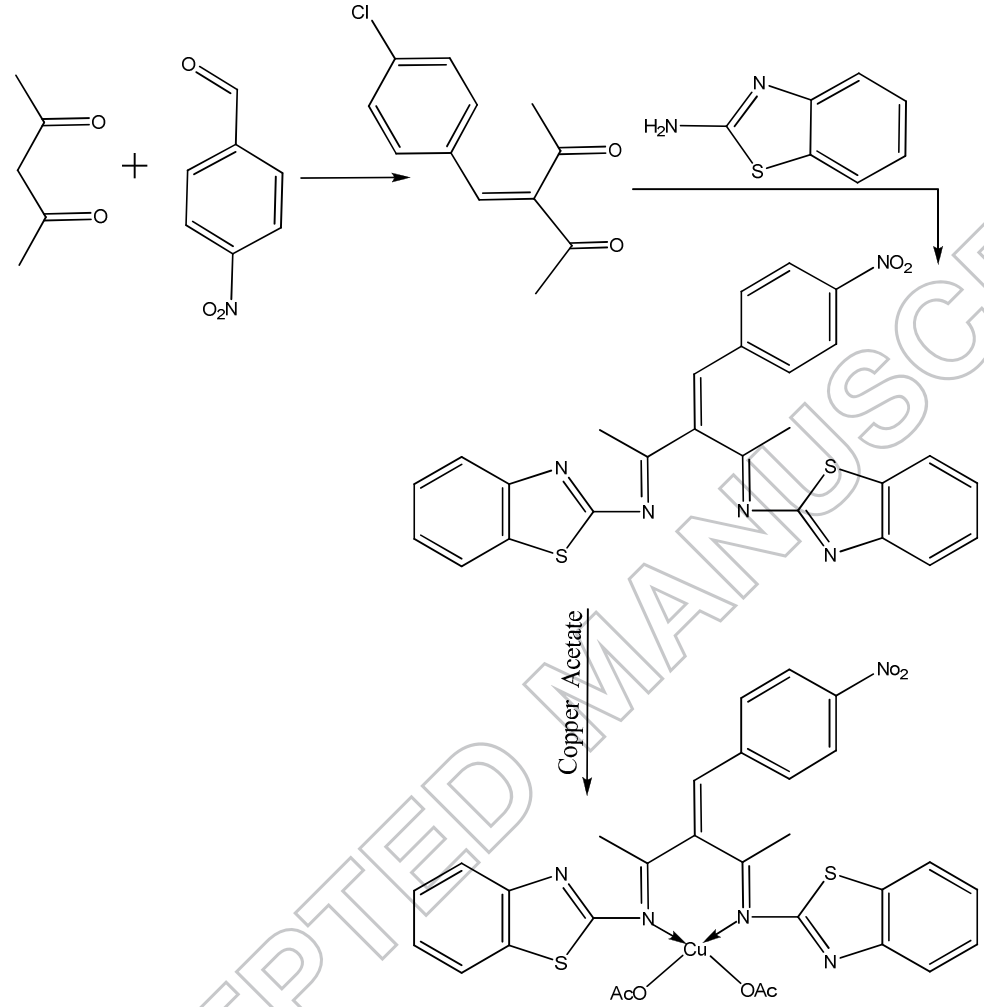

Scheme 2. Fragmentation pattern of the copper complex of L^1.

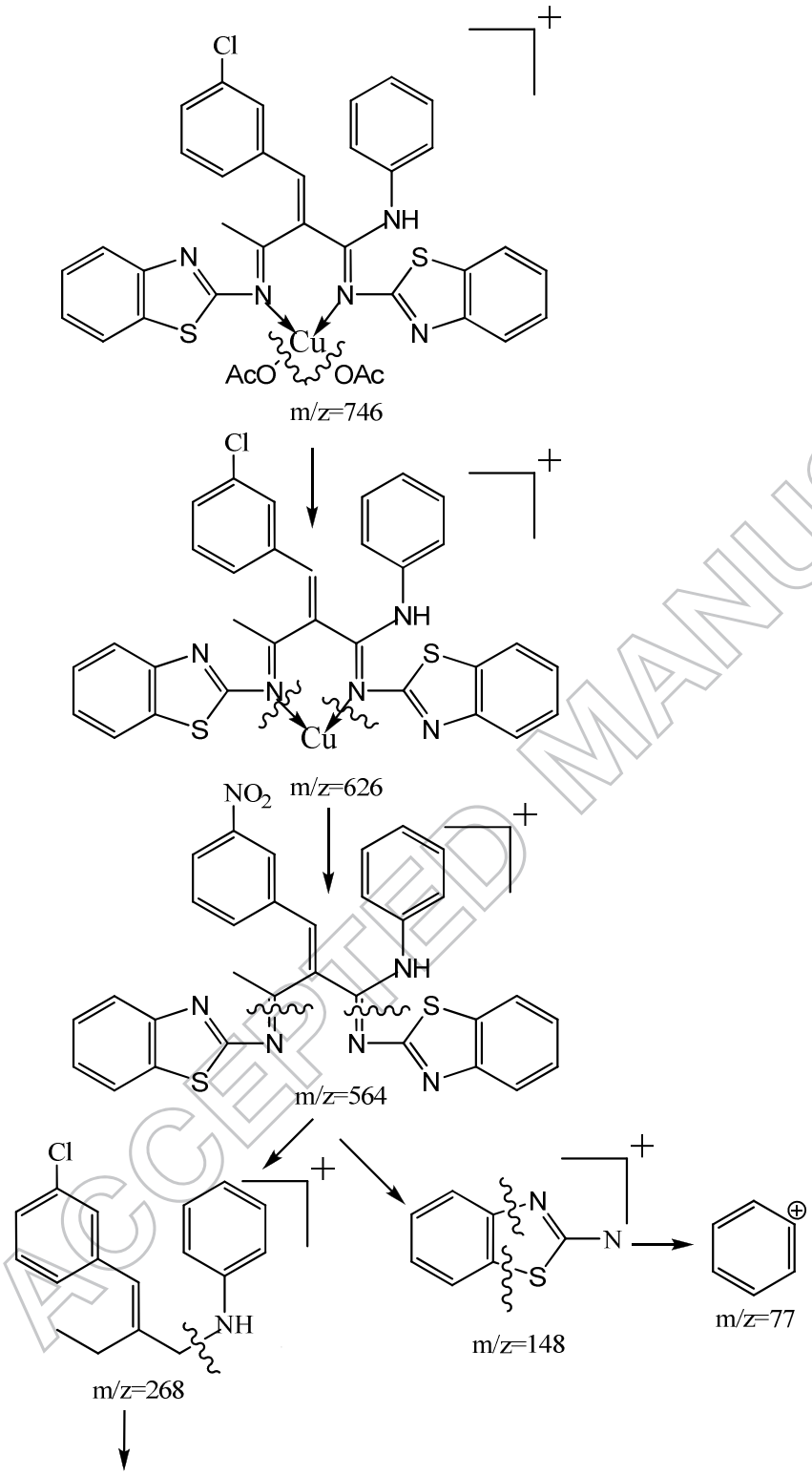

Scheme 2 (continued)

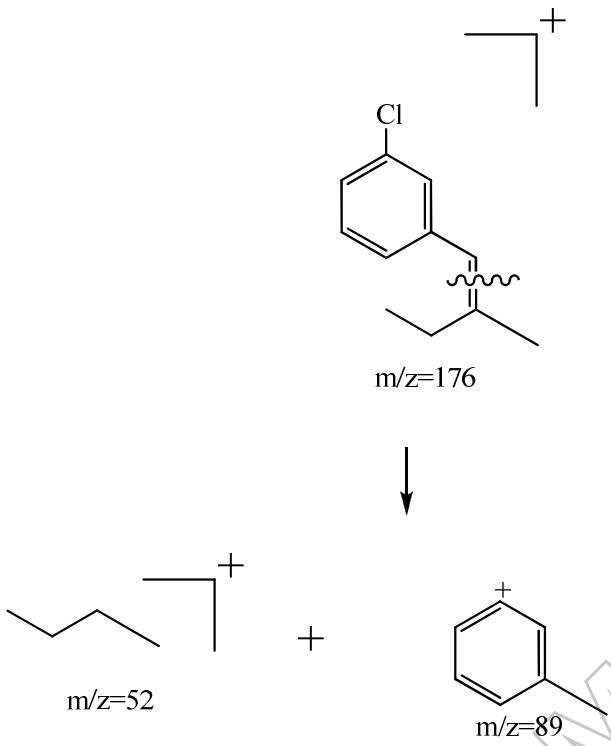

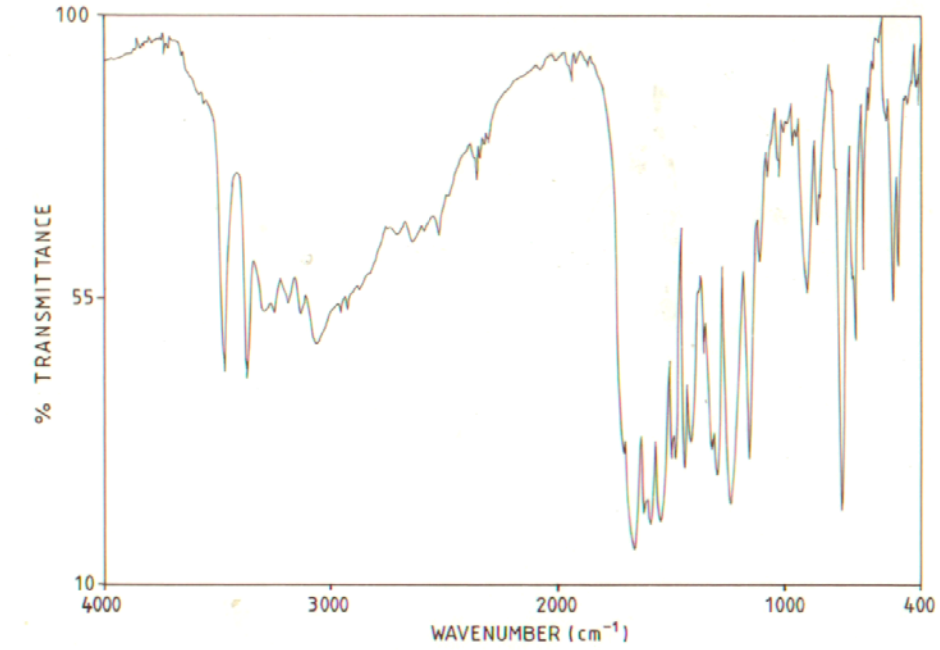

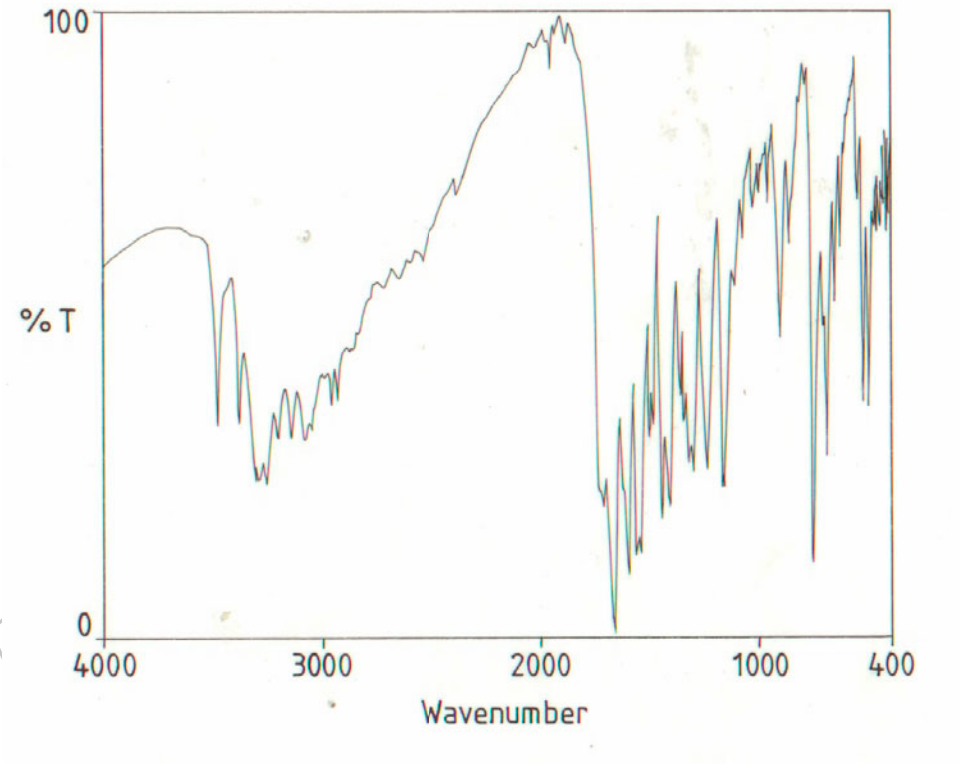

Figure 1. UV-Visible spectrum of L^1 and its copper complex in DMSO.

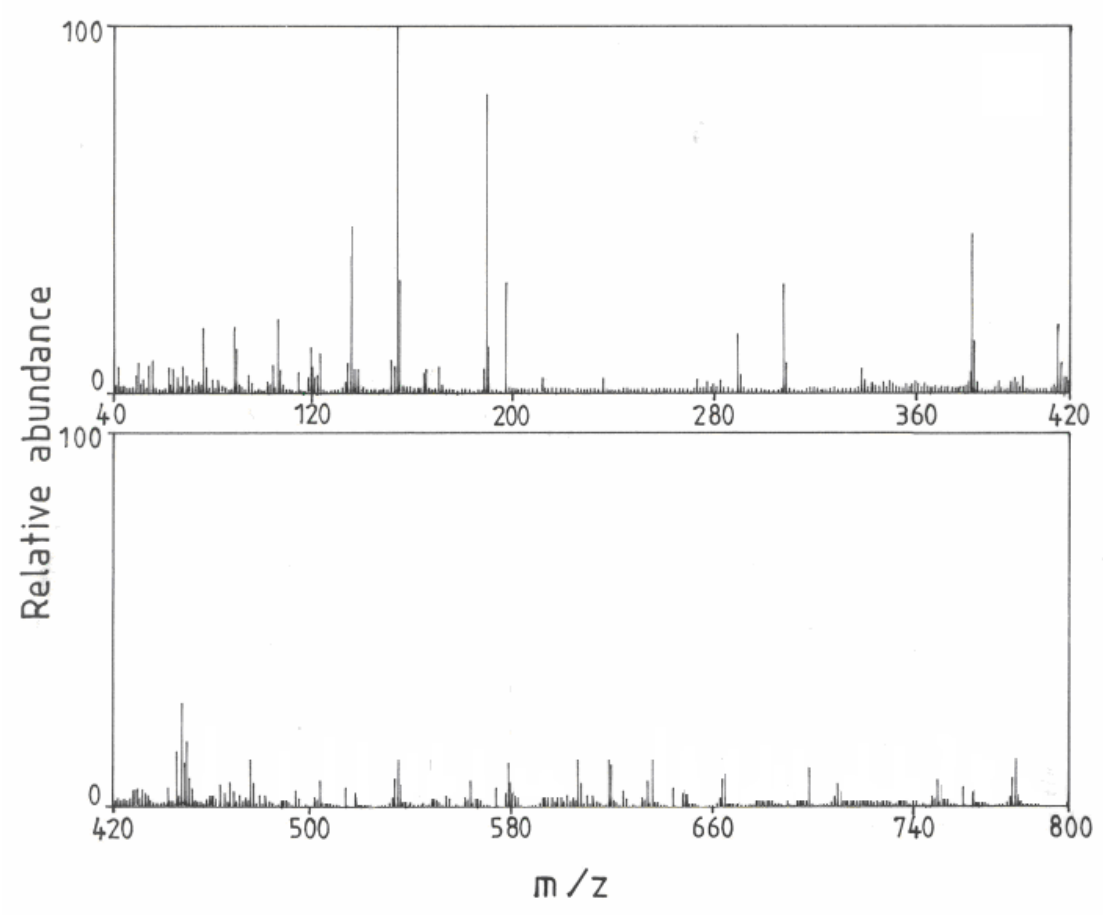

Figure 2. FAB mass spectra of L^1 and its copper complex.

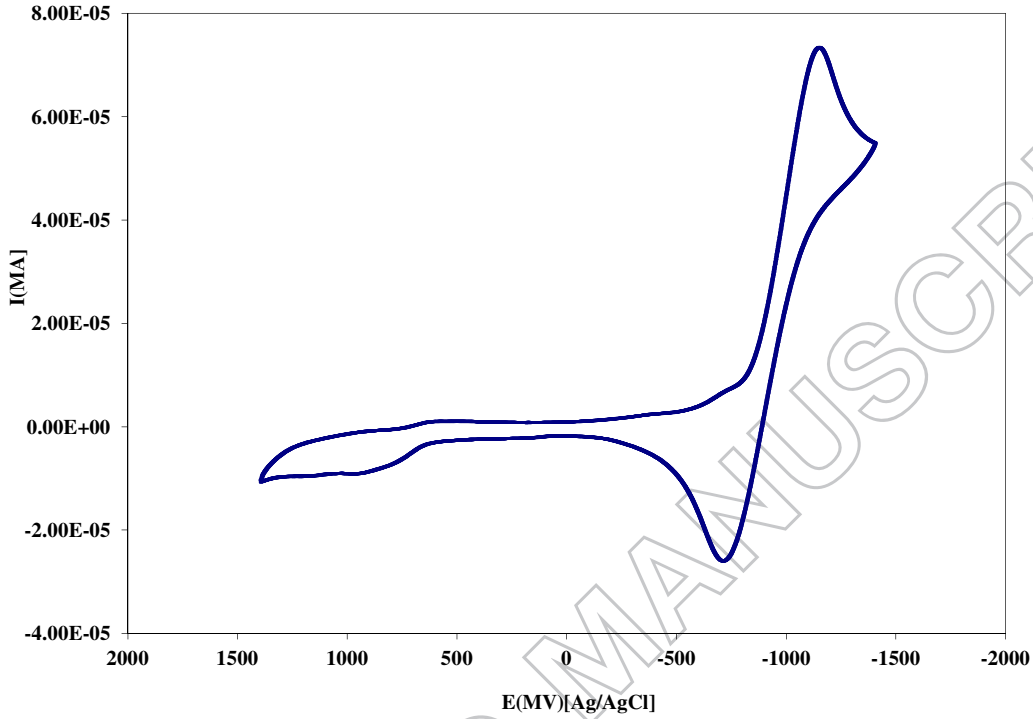

Figure 3. Cyclic voltammogram of the copper complex of L^1 in DMSO solution at room temperature.

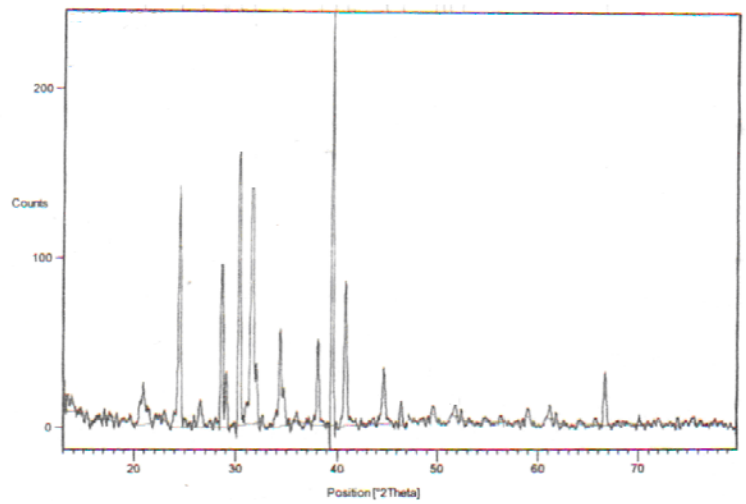

Figure 4. Powder XRD pattern of the copper complex of L^1.

Table 1. ESR spectral parameters for the copper complexes.

Complex	$g_{\parallel}$	$g_{\perp}$	g_{iso}	$A_{\parallel}$	$A_{\perp}$	$K_{\parallel}$	$K_{\perp}$	α^2	β^2	γ^2	$F=(g_{\parallel}/A_{\parallel})$
$[CuL^1(OAc)_2]$ at 300 K			2.06								
$[CuL^1(OAc)_2]$ at 77 K	2.22	2.06	-	156	44	0.84	0.52	0.70	1.6	0.76	145
$[CuL^2(OAc)_2]$ at 300 K			2.08								
$[CuL^2(OAc)_2]$ at 77 K	2.20	2.08	-	148	44	0.86	0.43	0.76	1.4	0.70	151
$[CuL^3(OAc)_2]$ at 300 K			2.12								
$[CuL^3(OAc)_2]$ at 77 K	2.26	2.05	-	158	52	0.74	0.49	0.81	1.3	0.82	143
$[CuL^4(OAc)_2]$ at 300 K			2.10								
$[CuL^4(OAc)_2]$ at 77 K	2.24	2.03	-	146	42	0.72	0.54	0.80	1.2	0.72	146

Table 2. Electrochemical parameters for the copper complexes.

Complex	E_{pa}	E_{pc}	ΔE_p	Potential assignment
$[CuL^1(OAc)_2]$	-0.154	-0.272	118	Cu(II)/Cu(I)
$[CuL^2(OAc)_2]$	-0.580	-0.730	150	Cu(II)/Cu(I)
	1.96	-		Ligand oxidation
$[CuL^3(OAc)_2]$	-0.620	-0.752	132	Cu(II)/Cu(I)
	0.465	-	-	Cu(II)/Cu(III)
$[CuL^4(OAc)_2]$	-0.606	-0.778	169	Cu(II)/Cu(I)
	0.436	-0.597	-	Cu(I)/Cu(0)

Table 3. Powder X-ray diffraction data for the copper complexes.

Complex	Grain size (nm)
$[CuL^1(OAc)_2]$	60
$[CuL^2(OAc)_2]$	66
$[CuL^3(OAc)_2]$	78
$[CuL^4(OAc)_2]$	52

Table 4. Minimum inhibitory concentration values of the synthesized compounds against the growth of bacteria (in μM).

Compound	*Staphylococcus aureus*	*Escherichia coli*	*Klebsiella pneumaniae*	*Pseudomonas aeruginosa*	*Proteus vulgaris*
L^1	0.58	0.76	0.62	0.72	0.68
L^2	0.76	0.82	0.68	0.80	0.90
L^3	0.74	0.70	0.72	0.84	0.88
L^4	0.68	0.74	0.46	0.52	0.76
$[CuL^1(OAc)_2]$	0.22	0.18	0.24	0.26	0.14
$[CuL^2(OAc)_2]$	0.36	0.22	0.28	0.34	0.20
$[CuL^3(OAc)_2]$	0.42	0.32	0.26	0.20	0.24
$[CuL^4(OAc)_2]$	0.14	0.20	0.22	0.10	0.16
Streptomycin	0.02	0.04	0.03	0.06	0.05

Table 5. Minimum inhibitory concentration values of the synthesized compounds against the growth of fungi (in μM).

Compound	*A. niger*	*A. flavus*	*C. albicans*	*R. stolonifer*	*R. bataicola*
L^1	0.84	0.88	0.72	0.68	0.62
L^2	0.58	0.70	0.80	0.76	0.68
L^3	0.62	0.76	0.72	0.84	0.90
L^4	0.82	072	0.80	0.78	0.84
$[CuL^1(OAc)_2]$	0.30	0.26	0.22	0.18	0.24
$[CuL^2(OAc)_2]$	0.26	0.28	0..20	0.18	0.24
$[CuL^3(OAc)_2]$	0.24	0.28	0.32	0.34	0.30
$[CuL^4(OAc)_2]$	0.18	0.22	0.16	0.24	0.20
Nystatin	0.04	0.02	0.08	0.06	0.1

Graphical abstract